processes

MDPI

Article

A Novel CEM-Based 2-DOF PID Controller for Low-Pressure Turbine Speed Control of Marine Gas Turbine Engines

Gun-Baek So

Department of Maritime Industry Convergence, Mokpo National Maritime University, 91 Haeyangdaehak-ro, Mokpo-shi 58628, Republic of Korea; sgb@mmu.ac.kr; Tel.: +82-10-9331-3608

Abstract: Gas turbine engines have several advantages over piston reciprocating engines, such as higher output per unit volume, reduced vibration, rapid acceleration and deceleration, high power output, and clean exhaust gases. As a result, their use for propulsion in ships has been steadily increasing. However, gas turbine engines exhibit significant parameter variations depending on the rotational speed, making the design of controllers to ensure system stability while achieving satisfactory control performance, a very challenging task. In this paper, a novel CEM-based 2-DOF PID controller design technique is proposed to ensure the stability of a gas turbine engine while improving tracking and disturbance rejection performance. The proposed controller consists of a PID controller focused on enhancing disturbance rejection performance and a set-point filter to improve tracking performance. The set-point filter is composed of gains from the controller and a single weighting factor. When tuning the gains of the controller, the maximum sensitivity is considered to maintain an appropriate balance between system stability and response performance. The key novelty of this study can be summarized in two main points. One is that the controller is designed by matching characteristic equations, and by setting the roots of the desired characteristic equation as multipoles, the gains of the PID controller can be tuned with only one adjusting variable, making the tuning of the 2-DOF controller easier. The other is that the controller parameters are tuned based on maximum sensitivity, thus taking into account the robust stability of the control system. To demonstrate the feasibility of the proposed method, simulations are conducted for four scenarios using various performance indices.

Keywords: gas turbine; PID controller; disturbance rejection; performance index

Citation: So, G.-B. A Novel CEM-Based 2-DOF PID Controller for Low-Pressure Turbine Speed Control of Marine Gas Turbine Engines. *Processes* **2024**, *12*, 1916. https://doi.org/10.3390/pr12091916

Academic Editors: Anthony Rossiter and Ján Piteľ

Received: 16 July 2024
Revised: 7 August 2024
Accepted: 4 September 2024
Published: 6 September 2024

1. Introduction

Gas turbine (GT) engines are being used in various industries [1–4], including the defense industry, and they have made significant advancements in their applications and performance. GT engines have a very high power output per unit volume compared to other existing thermal engines. Most maritime GT engines derived from aviation engines were initially applied to naval vessels. This is because, unlike commercial ships that prioritize cost-effectiveness, warships have unique performance requirements such as maximizing space for weapon systems, achieving maximum speed and high power capacity to support operational concepts, rapid acceleration, ensuring survivability through dense ship structures, and minimizing noise for anti-submarine warfare preparations. Therefore, the U.S. Navy's Zumwalt-class destroyers [5,6] adopted GT engines for their integrated power system, which manages both propulsion power and onboard service power.

In recent times, due to the strengthened environmental regulations led by the International Maritime Organization (IMO), such as the energy efficiency design index (EEDI) [7] and emission limits for nitrogen oxides (NOx) and sulfur oxides (SOx) [8], there has been an increasing demand for marine engines using fuels like LNG (liquefied natural gas), LPG (liquefied petroleum gas), methanol, and ammonia in commercial shipping. Furthermore, GT engine manufacturers are producing and supplying high-efficiency GT engines that

meet emission regulations for harmful exhaust gases, allowing them to be used in large cruise ships like the Queen Mary 2 [9] or high-speed ferries like the Francesco [10]. The performance requirements for commercial shipping are also changing with the increasing speed and cargo carrying capacity in maritime transportation.

Figures 1 and 2 are examples of electric propulsion ships powered by gas turbine generators. The Zumwalt-class destroyer [5,6] is equipped with two 35.4 MW main turbine generators and two 3.8 MW auxiliary turbine generators. The cruise ship Queen Mary 2 [9] is equipped with two 25 MW turbine generators and four 16.8 MW diesel generators.

Figure 1. The Zumwalt-class destroyer.

Figure 2. The cruise ship Queen Mary 2.

As a result of these changes, GT engines that were initially primarily applied in naval vessels are now increasingly being utilized in commercial shipping such as LNG carriers, cruise ships, and offshore facilities like floating production storage offloading units [11].

The performance of GT engines can be maintained by appropriately adjusting the engine's rotational speed and the temperature, pressure, and other parameters at each station to prevent issues like air pulsations and vibrations generated by the axial compressor rotor system when changing the rotational speed. To achieve this, it is essential to design a precise rotational speed controller that can receive feedback from sensors such as the engine's rotational speed, maximum temperature, and pressure at each station in order to supply fuel oil and air stably to the combustor. Generally, modeling of the control target process is necessary to design the controller, and many controllers are designed based on such models. Numerous studies on modeling [12–20] and control system design [21–30] for various gas turbine engines have been reported in the literature so far.

The most widely used GT model is Rowen's models [12] developed for power system stability studies. Each model is represented simply in block diagrams. The fuel preparation system is represented by two consecutive first-order transfer functions with internal loop gains. Time delay is considered in the combustor. This model consists of transfer functions, integrators, constant gains, and saturators. Hussain et al. [13] derived a simplified physical

model for a single-shaft GT based on the principles of mass and energy conservation in thermodynamics. The results of the simplified model showed similar responses to several load variations compared to the manufacturer's model. In the study by Yee et al. [14], a validated model of GT primarily based on thermodynamic principles was presented. However, some parameters were determined by calculating the temperature difference at a steady state between the turbine and compressor, thus exhibiting highly nonlinear variations. Chaibakhsh et al. [15] developed an analytical model for GT engines, applying the principles of mass and energy conservation. The parameters of the model were identified using a genetic algorithm (GA), which is a nonlinear optimization technique. Cha et al. [16] developed a mathematical model capable of simulating the dynamic behavior of two-spool GT engines for marine propulsion systems. The engine performance model was developed using data provided by the engine manufacturer. Simulink was used to model dynamic behavior, and validation was performed by comparing performance data obtained from the manufacturer under steady-state conditions with the mathematical model. Mohamad et al. [17] derived a simple physical model for a GT power generation system based on thermodynamic principles. The model parameters were identified through the optimization technique of genetic algorithms. Adjustment of the fuel flow rate is achieved through a combination of control valve and pilot valve operations. Aygun and Turan [18] used a genetic algorithm to model the exergetic parameters of a turbofan engine during the cruise phase, enhancing accuracy over the least squares method and determining optimal cruise flight conditions. Xu et al. [19] proposed an input and output self-tuning hybrid model to overcome the limitations of traditional gas path models for GT engines. The effectiveness of this model was demonstrated through simulations and actual tests. Yang et al. [20] reviewed 70 years of simulation, heat transfer effects, and platform developments for the transient performance analysis of gas turbines. The limitations of white-box and black-box approaches and numerical methods were presented, highlighting the need for developing complex heat transfer models.

A technique commonly found in the literature for gas turbine control is model predictive control (MPC) strategy [21]. MPC has been widely utilized in control applications such as power plants and similar systems. This is because it can naturally handle operational constraints and apply optimization to future signals. Sáez et al. [22] proposed a GA-based fuzzy predictive control strategy for controlling GT. In the initial design, the parameters were assumed to be constant, and in the second design, they were updated using GA based on each prediction. Hou et al. [23] proposed a fuzzy predictive strategy for controlling the GT in a combined cycle GT system. Here, the fuzzy predictive controller provides optimal set-points for the fuel flow rate and inlet guide vane to control the GT. To validate the effectiveness of the fuzzy predictive strategy, extensive comparative analyses with other techniques were provided. Bonfiglio et al. [24] employed sliding mode control (SMC) as a different approach from MPC for GT control, where the control law signals are directly applied to the GT system. This method has shown promising performance for various load variations with faster responses compared to traditional PID controllers. Mohamed and Khalil [25] conducted a comprehensive review of the modeling, identification, and control of gas turbine power generation plants. They systematically analyzed various approaches and techniques, discussing models that capture key dynamic changes, neural network models, and mathematical models used in stability studies. Zhou et al. [26] proposed an improved multivariable generalized predictive controller algorithm for the direct control of gas turbine engines. The adaptive component-level model and recursive least squares algorithm were used to estimate and identify the performance parameters. A penalty factor was added to the cost function for limit protection. In the study by Hou et al. [27], a fuzzy modeling approach and a fast model predictive control algorithm were introduced to address the complex characteristics of GT systems. Entropy-based clustering and subspace identification were used to identify the system model. Lin et al. [28] studied the controller design for micro GT in power generation. A nominal nonlinear model integrating a startup model and component characteristic map model was implemented. Nonlinear and linear

active disturbance rejection controllers and PID controllers were designed to achieve speed and load tracking control.

Ryu [29] proposed a PID speed controller for the high-pressure turbine of a marine LM-2500 GT engine using the GA technique. Lee et al. [30] designed an IMC-based PID controller for the high-pressure turbine of a marine LM-2500 GT engine. This method exhibited superior performance in both set-point tracking and disturbance rejection responses. Additionally, there have been various studies reported in the literature on the design of PID controllers based on process models. Skogestad [31] proposed a SIMC method for controlling various processes with time delays. This method has been widely utilized by many control system designers as a benchmark control algorithm for validating the effectiveness of their proposed methods.

Despite these various research efforts, there are still challenges that need to be addressed, for example, parameter variations due to transitions between operating points, the integration of multiple controllers designed for different operating points, and control of the airflow rate in the compressor during combustion. Furthermore, research is needed to ensure the stability of control systems and develop controllers with improved speed control performance. In general, the most desirable control system is one with a simple structure that can achieve excellent performance and robustness with minimal adjustment variables for tuning the controller parameters. Therefore, this study proposes a simple structured 2-DOF PID controller that ensures the stability of the LM2500 GT system installed on naval ships while providing excellent set-point tracking and disturbance rejection performance over a wide operating range. The proposed controller consists of a PID controller and a set-point filter. The PID controller is designed with a focus on disturbance rejection, while the set-point filter is designed to improve the set-point tracking performance. Furthermore, when tuning the parameters of the PID controller, the maximum sensitivity (MS), which is the maximum value of the sensitivity function, is considered as a stability index.

The proposed controller is applied to the speed control of the low-pressure turbine in the GT system, and its effectiveness is validated through simulation compared to traditional control methods.

The structure of this paper is as follows: In Section 2, the GT engine, along with a fuel oil metering unit (FMU), is modeled as a third-order plus time delay (TOPTD) system for speed control, and it is approximated as a first-order plus time delay (FOPTD) model for controller design. Section 3 describes the core of the research, which is the design of the 2-DOF PID controller based on the CEM (characteristic equation matching) technique. Section 4 conducts simulations to validate the effectiveness of the proposed controller under nominal conditions and parameter uncertainties. Finally, in Section 5, the conclusions are summarized.

2. Modeling of the Marine LM2500 Gas Turbine Engine System

2.1. Structure of the Marine LM2500 GT Engine

The marine LM2500 propulsion GT engine, which is commonly installed on naval vessels, is a two-spool turbo-shaft engine derived from aviation engines like the TF39 and CF6-6, adapted for maritime use. As for the key specifications of this engine, the output is approximately 21 megawatts, the LPT rotational speed ranges from about 1100 to 3000 rpm, the displacement of the fuel oil metering valve (FMV) spool ranges from 0 to 22 mm, and the average fuel consumption is 269.5 g/kWh.

This engine consists of components such as a gas generator, low-pressure turbine (LPT), fuel oil pump, FMU, hydraulic pump, variable stator vane actuator (VSVA), and starter, as depicted in Figure 3. The gas generator consists of an axial flow high-pressure compressor, a high-pressure turbine (HPT) to drive it, and a combustor. The LPT is used to directly generate propulsion power by rotating the propeller shaft. The HPT and LPT are mechanically separated.

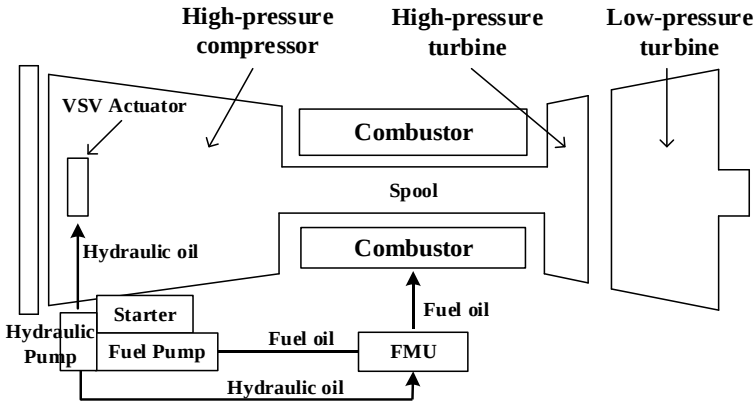

Figure 3. Structure of the LM2500 GT engine.

2.2. Modeling of the LM2500 GT Engine

Modeling is crucial for accurately implementing algorithms in control systems by finely reflecting the characteristics that arise during various operating conditions of the plant. In this study, modeling is conducted by dividing it into the fuel system and the combustor-LPT system, as shown in Figure 3. To facilitate symbol differentiation, transfer functions are represented in uppercase, while signals are represented in lowercase.

In Figure 4, $u(s)$, $z(s)$, and $y(s)$ represent the output of the controller, output of FMU, and rotational speed of LPT, respectively. $P_{FMU}(s)$ and $P_E(s)$ represent the transfer functions of FMU and combustor-LPT system.

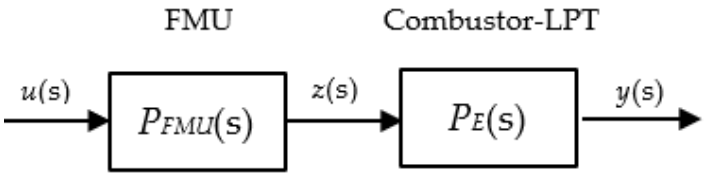

Figure 4. Open-loop block diagram of the LM2500 GT engine system.

The FMU of the fuel oil system is modeled as a second-order system, while the combustor-LPT system is modeled as a FOPTD system using actual operating data. This results in deriving the overall GT system as a TOPTD system.

The FMU consists of a FMV that includes an actuator—specifically, a torque motor-servo valve—along with a displacement transducer, internal amplifier, and linear variable differential transformer (LVDT), as shown in the operational mechanism in Figure 5.

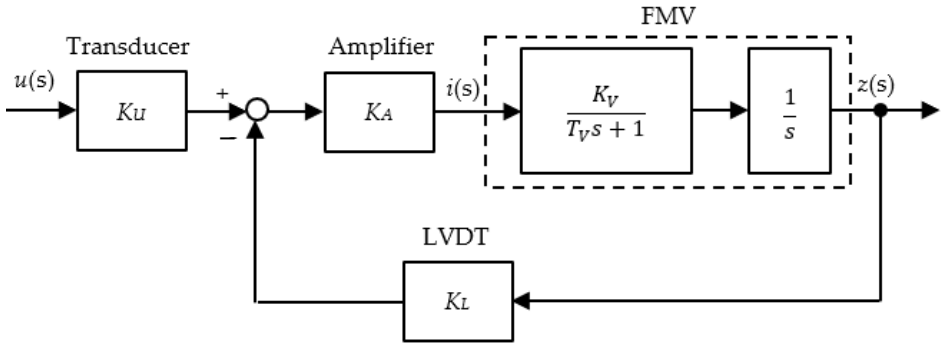

Figure 5. Block diagram of an FMU.

In Figure 5, $i(s)$ and $z(s)$ represent the output of the internal amplifier and spool displacement of the FMV. K_U, K_A, K_L, K_V, and T_V represent the gain of the transducer, gain of the internal amplifier, gain of the LVDT, the steady-state gain, and time constant of the FMV, respectively.

The FMV [16,29,30] is represented as a second-order system with an integrator, as shown in Equation (1).

$$\frac{z(s)}{i(s)} = \frac{K_V}{s(T_V s + 1)} \tag{1}$$

The closed-loop transfer function of the FMU can be expressed as Equation (2).

$$P_{FMU}(s) = \frac{z(s)}{u(s)} = \frac{K_U K_A K_V}{T_V s^2 + s + K_A K_V K_L} \tag{2}$$

The values of K_V and T_V were taken from [16,29,30], and the K_L value of the LVDT was set to 0.8, as it converts the spool displacement of 20 mm to 4–20 mA. By matching the value of K_U with K_L, the steady-state gain of the FMU was 1. Additionally, the value of K_A was selected by simulating the step response of the FMU multiple times to find an appropriate value. Table 1 summarizes the parameters of the FMU within Figure 5.

Table 1. Parameters of the FMU.

Parameters	K_U	K_A	K_L	K_V	T_V
Values	0.8	2	0.8	4	0.1

The combustor-LPT system is modeled mathematically because it directly generates propulsion power for GT-driven ships. The integrated transfer function $P_E(s)$ of the combustor-LPT system, as a ratio of the LPT rotational speed $y(s)$ to the FMV spool displacement $z(s)$, can be expressed as Equation (3).

$$P_E(s) = \frac{y(s)}{z(s)} = \frac{K_E}{T_E s + 1} e^{-L_E s} \tag{3}$$

where K_E and T_E, respectively, represent the steady-state gain and time constant of the LPT system, including the combustor.

L_E represents the time delay, accounting for the time it takes for the fuel oil adjusted in the FMU to reach the combustor and the time for the ignited combustion gases from the combustor to reach the blades of the LPT via the HPT.

By combining Equations (2) and (3), the mathematical model of the entire GT system can be summarized as Equation (4).

$$P(s) = \frac{y(s)}{u(s)} = \frac{K_U K_A K_V K_E}{(T_V s^2 + s + K_A K_V K_L)(T_E s + 1)} e^{-L_E s} = \frac{b_0}{a_3 s^3 + a_2 s^2 + a_1 s + a_0} e^{-L_E s} \tag{4}$$

where a_3, a_2, a_1, a_0, and b_0 are as follows:

$$a_3 = T_V T_E,\ \ a_2 = T_V + T_E,\ \ a_1 = K_A K_V K_L T_E + 1,\ \ a_0 = K_A K_V K_L, \text{ and } \ b_0 = K_U K_A K_V K_E$$

2.3. Parameter Estimation of the Models

Equation (3) represents a GT engine in which the parameters can vary significantly depending on the operating region. Therefore, the parameters are estimated for three operating regions within the combustor-LPT system: low-speed, medium-speed, and high-speed. The models for the low-speed, medium-speed, and high-speed operating regions correspond to steady-state speeds of 1600, 2200, and 2800 rpm, respectively. To obtain the dynamic characteristics of the mathematical model, operational data obtained from the LM2500 GT installed on naval ships are used. Figures 6–8 represent the fuel flow rate, FMV spool position, and time delay with respect to the rotational speed of the LPT.

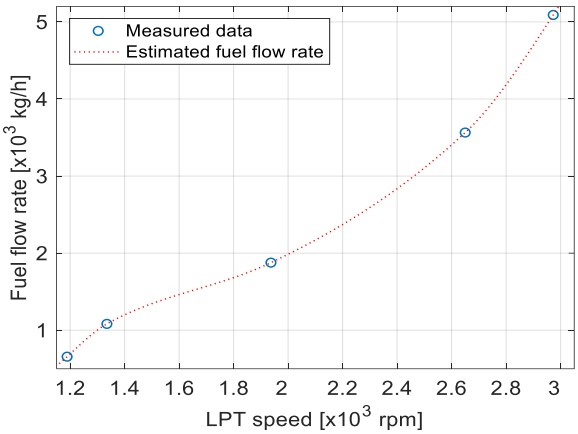

Figure 6. The fuel flow rate with respect to the LPT speed.

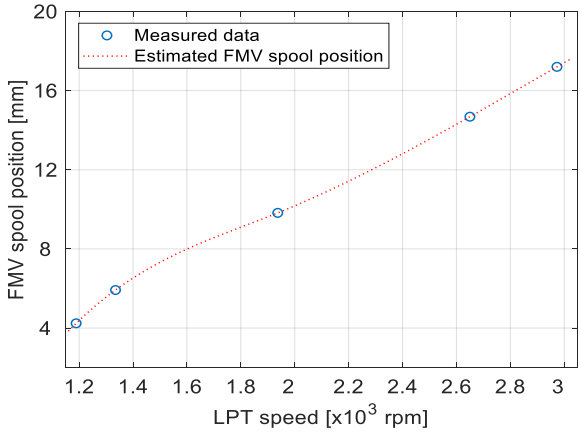

Figure 7. The FMV spool position with respect to the LPT speed.

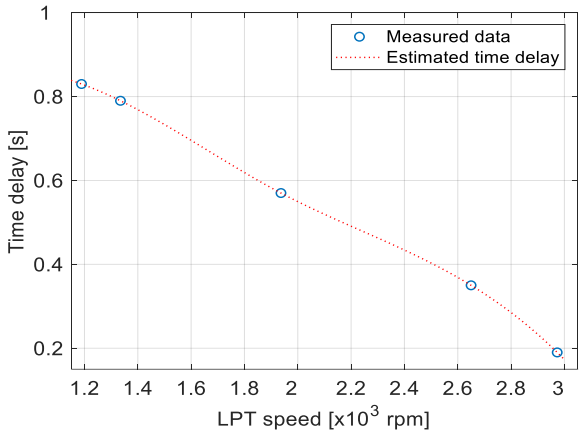

Figure 8. The time delay with respect to the LPT speed.

In Figures 6–9, the results were averaged after changing the set-points of the rotational speed multiple times for the five operating points and were approximated with reference to the commissioning data. Here, the fuel flow rate and FMV spool position are the values at the steady state. The time delay was appropriately assumed by referencing the length and diameter of the fuel pipeline from the spool valve to the combustor, as well as the fuel flow rate. Figure 9 represents the relationship between fuel flow rate and FMV spool position.

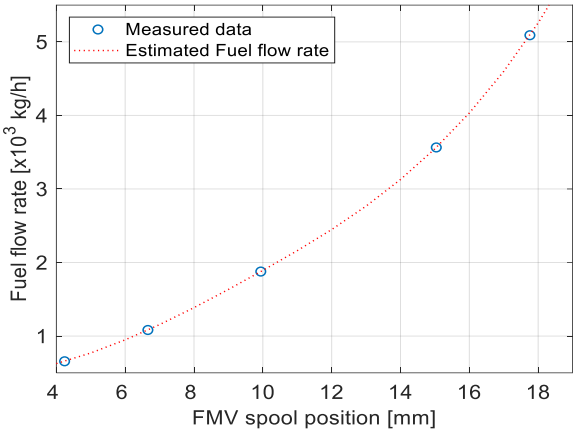

Figure 9. The fuel flow rate with respect to the FMV spool position.

The estimated parameters through the spline interpolation method [32] for each operating region in Figures 6–9 are summarized in Table 2. However, the time constants were appropriately estimated and selected based on prior research [29,30].

Table 2. Parameters of the LM2500 GT engine.

Parameters	K_E	T_E	L_E
Low-speed region, P_{E1}	200.3	5.65	0.69
Medium-speed region, P_{E2}	192.6	3.97	0.49
High-speed region, P_{E3}	176.7	2.30	0.28

The entire GT system is represented as a TOPTD system, and by substituting the coefficients from Tables 1 and 2 into Equation (4), the transfer functions $P_i(s)$ (i = 1, 2, 3) of the GT system at each operating point are obtained as shown in Equations (5a)–(5c).

$$P_1(s) = \frac{1281.92}{0.565s^3 + 5.75s^2 + 37.16s + 6.4} e^{-0.69s} \tag{5a}$$

$$P_2(s) = \frac{1232.64}{0.397s^3 + 4.07s^2 + 25.408s + 6.4} e^{-0.49s} \tag{5b}$$

$$P_3(s) = \frac{1130.88}{0.23s^3 + 2.4s^2 + 14.72s + 6.4} e^{-0.28s} \tag{5c}$$

2.4. Approximation of the Models

In the previous section, the GT system was divided into three operational regions, each of which was modeled as a third-order system with a time delay. Among these, it is considered reasonable to use the model of the medium-speed region for controller design. Therefore, the medium-speed model is selected as the standard model for controller design and approximated as a FOPTD model, as shown in Equation (6).

$$M(s) = \frac{K}{Ts + 1} e^{-Ls} \tag{6}$$

where K, T, and L represent the steady-state gain, time constant, and time delay of the FOPTD model, respectively. The unit step response of the TOPTD system in the medium-speed region is obtained, and the process reaction curve (PRC) method [33] is used to identify the parameters of the FOPTD model from this response. In the PRC method, the first step is to calculate the times at which the unit step response reaches 28.3% and 63.2% of the steady-state value. The next step is to calculate the difference between these two times and multiply it by 1.5 to obtain the FOPTD model's time constant T. Then, the time delay

L is determined by subtracting this time constant T from the time at which the response reaches 63.2% of the steady-state value. The gain K is the magnitude of the steady-state response to a unit step input. Table 3 summarizes the parameters of the FOPTD model obtained using the PRC method.

Table 3. Parameters of the FOPTD model.

Parameters	***K***	***T***	***L***
Values	192.6	3.97	0.64

Figure 10 shows the unit step responses of the original TOPTD system and FOPTD model, along with the error between them.

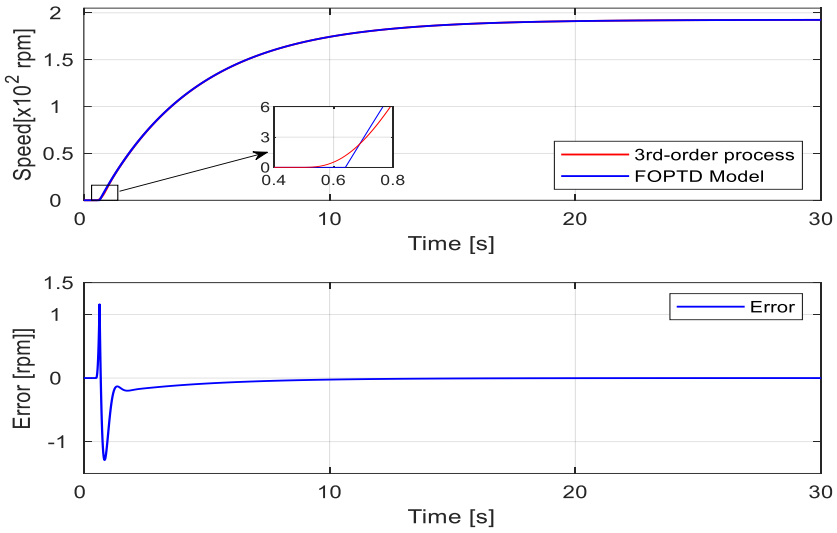

Figure 10. Comparison of the step responses between the TOPTD GT System and FOPTD model.

As you can see in Figure 10, the FOPTD model closely matches the original TOPTD system with a maximum error of around 1.3 rpm. This indicates that the FOPTD model is suitable for controller design.

3. Design of the Proposed Controller

The proposed CEM-based 2-DOF PID controller consists of a novel PID controller $C(s)$ and a set-point filter $F_r(s)$, as shown in Figure 11.

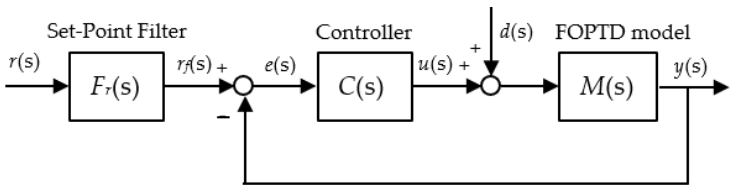

Figure 11. Structure of the CEM based 2-DOF PID control system.

where $r(s)$, $r_f(s)$, $e(s)$, $u(s)$, y(s), and $d(s)$ represent the reference input, output of the set-point filter, error, output of the controller, output of the model, and disturbance input, respectively. $F_r(s)$, $C(s)$, and $M(s)$ represent the transfer functions of the set-point filter, PID controller, and FOPTD model, respectively.

3.1. CEM-Based PID Controller

The proposed CEM technique is a form of the pole placement method in control system design that analytically designs the controller parameters by aligning the characteristic

equation of the closed-loop system transfer function with that of the desired closed-loop transfer function. When selecting the desired characteristic equation, the characteristic roots are placed to be multiple roots to simplify controller design and tuning.

The transfer function of the PID controller is given by Equation (7), and the model used for controller design is a stable FOPTD model approximated as Equation (6).

$$C(s) = K_p + \frac{K_I}{s} + K_D s \tag{7}$$

where K_P, K_I, and K_D represent the proportional gain, integral gain, and derivative gain of the PID controller, respectively.

In the control system depicted in Figure 11, the relationship between the reference input $r(s)$, disturbance input $d(s)$, and the output $y(s)$ of the controlled process is given by Equation (8).

$$y(s) = \frac{F_r(s)C(s)M(s)}{C(s)M(s)+1} r(s) + \frac{M(s)}{C(s)M(s)+1} d(s) \tag{8}$$

By setting the denominator of the closed-loop transfer function of the system to zero and substituting Equations (6) and (7) into it, the characteristic equation represented by Equation (9) is derived.

$$1 + C(s)M(s) = 1 + \left(K_P + \frac{K_I}{s} + K_D s\right) \frac{K}{Ts+1} e^{-Ls} = 0 \tag{9}$$

By approximating the time delay term as $e^{-Ls} \approx \frac{1-0.5Ls}{1+0.5Ls}$ using a first-order Pade approximation, it can be rearranged and expressed as Equation (10).

$$\alpha s^3 + \beta s^2 + \gamma s + 1 = 0 \tag{10}$$

where α, β, and γ are as follows:

$$\alpha = \frac{0.5LT}{KK_I} - \frac{0.5LK_D}{K_I},\ \beta = \frac{T - 0.5L}{KK_I} + \frac{K_D - 0.5LK_P}{K_I},\ \text{and}\ \gamma = \frac{1}{KK_I} + \frac{K_P}{K_I} - \frac{L}{2}.$$

Since the characteristic equation of the closed-loop transfer function is of the third order, the desired characteristic equation for controller design is also chosen to be of the third order, as shown in Equation (11).

$$(\lambda s + 1)^3 = 0 \tag{11}$$

By equating the coefficients of each order in the characteristic Equation (10) with those in the desired characteristic Equation (11), three equations are formed. Solving these equations results in the three parameters of the PID controller, as shown in Equations (12a)–(12c).

$$K_P = \frac{L^3 + (6\lambda + 4T)L^2 - 12\left(\lambda^2 - 2T\lambda\right)L - 8\lambda^3}{K(L+2\lambda)^3} \tag{12a}$$

$$K_I = \frac{4L(L+2T)}{K(L+2\lambda)^3} \tag{12b}$$

$$K_D = \frac{TL^3 + 6T\lambda L^2 - 4(2\lambda - 3T)\lambda^2 L - 8T\lambda^3}{K(L+2\lambda)^3} \tag{12c}$$

As shown in Equations (12a)–(12c), K, T, and L are determined from the FOPTD model used for controller design. Therefore, it can be observed that the only variable that the user needs to adjust is the time constant λ in the desired characteristic equation.

3.2. Set-Point Filter

The PID controller in Equations (12a)–(12c) is designed with a focus on disturbance rejection, which can result in a large overshoot, depending on the set-point value. To reduce this overshoot, the controller output of Equation (13) is used.

$$u(t) = K_P(br(t) - y(t)) + K_I \int_0^t (r(\tau) - y(\tau))d\tau + K_D\left(\frac{dr(t)}{dt} - \frac{dy(t)}{dt}\right) \tag{13}$$

where b is a weighting factor that takes values between 0 and 1.

By performing the Laplace transform on Equation (13) to obtain the transfer function of the set-point filter $F_r(s)$, it can be expressed as Equation (14).

$$F_r(s) = \frac{r_F(s)}{r(s)} = \frac{K_D s^2 + bK_P s + K_I}{K_D s^2 + K_P s + K_I} \tag{14}$$

3.3. Controller Parameter Tuning

The adjustment variable for tuning the parameters of a CEM-based PID controller, as can be seen in Equations (12a)–(12c), is only the time constant λ of the desired characteristic equation. The three parameters of the PID controller are tuned based on the MS, such as Equation (15), which represents the maximum value of sensitivity function that can appropriately compromise between responsiveness and stability.

$$\mathrm{MS} = \max_{\omega} \left| \frac{1}{1 + C(j\omega)M(j\omega)} \right| \tag{15}$$

When the MS value is large, the disturbance rejection response is excellent but the stability deteriorates. On the other hand, when the MS value is small, the opposite occurs. Typically, for a stable FOPTD model, the controller is designed to have a MS value in the range of 1.4 to 2.0 [34]. In this paper, the design $\mathrm{MS_d}$ of 1.7 is specified for a system composed of the FOPTD model and PID controller, taking into account the system's stability and performance. Therefore, to achieve $\mathrm{MS_d}$ = 1.7, the desired time constant λ was adjusted to 0.7801 for tuning the parameters of the PID controller. The results, along with the parameters of the Lee-IMC controller and Skogestad's SIMC controller for comparison, are summarized in Table 4. The actual $\mathrm{MS_a}$ represents the MS obtained with the PID controller and the original TOPTD system. Therefore, when calculating the actual $\mathrm{MS_a}$ from Equation (15), the TOPTD system $P_2(j\omega)$ is used instead of the model $M(j\omega)$.

Table 4. Parameter tuning for the controllers.

Tuning Methods	Parameters				Remarks	
	K_P	K_I	K_D	λ	$\mathbf{MS_a}$	$\mathbf{MS_d}$
Proposed	0.0233	0.01071	0.00473	0.7801	1.7482	1.700
SIMC	0.0161	0.00405	-	0.6400	1.6117	1.590
Lee-IMC	0.0219	0.00510	0.00648	0.6965	1.7492	1.699

4. Simulation

Figure 12 depicts the entire control system composed of set-point filter, PID controller, FMU, saturator, and combustor-LPT. Considering the limitation on the maximum displacement of the actual FMV spool, a saturator with a limitation of 22 mm is taken into account.

The simulation is conducted for the original TOPTD system under the nominal condition and parameter uncertainty conditions using the proposed method. The nominal condition refers to the TOPTD system in the medium-speed operating region, as the controller was designed for this operating region. The parameter uncertainty condition refers to the TOPTD systems in the low-speed and high-speed operating regions. Additionally,

simulations are also conducted for a parameter uncertainty model where K_E and L_E are increased by 5% each and T_E is decreased by 5% for the GT system in the medium-speed operating region. When conducting simulations in the low-speed region, medium-speed region, and high-speed region, the weighting values of the set-point filter are adjusted to 0.3, 0.62, and 0.79, respectively.

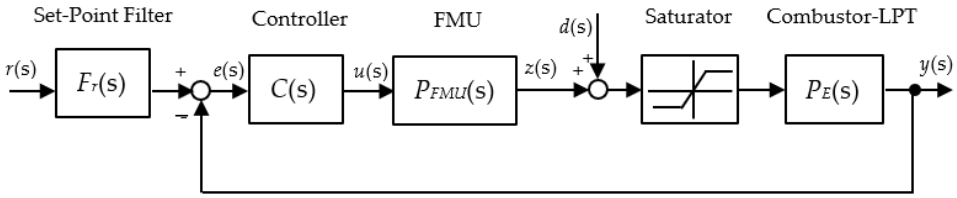

Figure 12. An overall control system for speed control of a GT engine.

Performance is quantitatively compared in each simulation based on the integral of time-weighted absolute error (*ITAE*), taking into account parameters such as 2% settling time T_s, peak response value M_{peak}, and 2% recovery time T_{rcy}.

$$ITAE = \int_0^t \tau|e(\tau)|d\tau \tag{16}$$

Furthermore, the system's stability is evaluated through the stability evaluation index MS_a. The performance of the controller is considered superior and more stable when these performance indices have smaller values. The proposed controller is compared with the responses of the Lee-IMC and SIMC controllers.

4.1. Medium-Speed Operating Region

Figure 13 depicts the responses for the nominal state condition when the LPT is initially rotating at 1600 rpm, a step input of 2200 rpm is applied at t = 0 s, and disturbance inputs are introduced at t = 20 s. In this scenario, the disturbance assumes that wind corresponding to 30% of the current load is applied as a step input in a vertical manner to the bow of the naval vessel. When operating at 2200 rpm, the position of the FMV spool is approximately 11.4 mm. Therefore, using Figure 9 to convert the current load to fuel flow rate, it corresponds to approximately 2280 kg/h, and external disturbances due to wind result in an additional fuel oil quantity of about 684 kg/h.

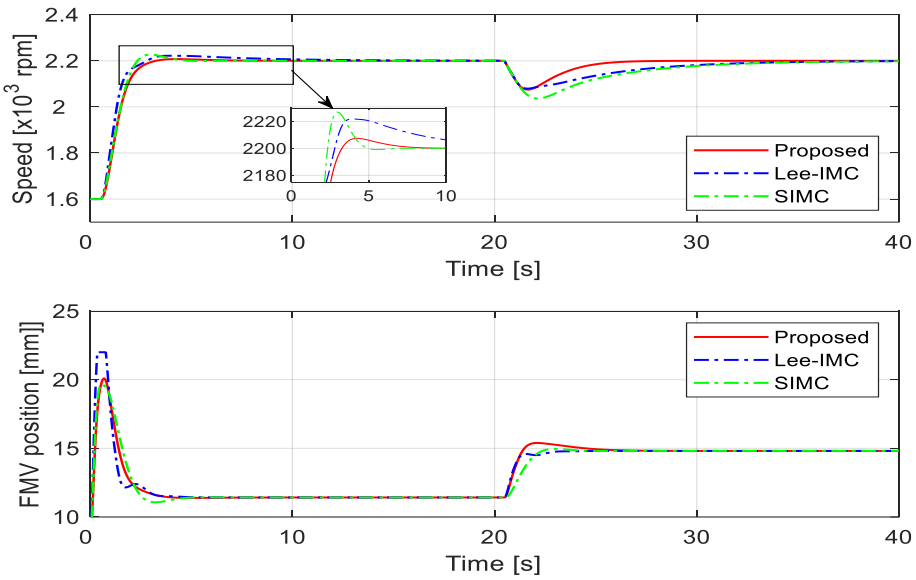

Figure 13. Step responses and FMV spool position for the medium-speed region.

Table 5 summarizes the performance indices for the proposed controller and the controllers used for comparison.

Table 5. Performance comparisons for the medium-speed operating region.

Tuning Methods	Tracking Performance			Disturbance Performance			MSa
	T_s	M_{peak}	$ITAE_s$	T_{rcy}	M_{peak}	$ITAE_d$	
Proposed	2.817	7.502	716.8	7.011	124.9	919.3	1.748
SIMC	3.887	27.000	717.9	17.650	163.6	4256.1	1.612
Lee-IMC	7.471	21.883	1463.1	18.069	121.0	3418.8	1.749

In the set-point tracking response, among the three methods, the proposed controller exhibits the smallest T_s, $ITAE_s$, and M_{peak}, making it the most superior in terms of all performance indices. The SIMC method has a similar level of $ITAE_s$ to the proposed approach but has a significantly larger M_{peak}. The Lee-IMC method has the largest T_s and $ITAE_s$. In particular, for Lee-IMC, it can be observed that, in the set-point tracking response, the initial control input is too large, causing the displacement of the FMV spool to reach the limit of 22 mm. In the disturbance rejection response, the proposed controller shows excellent performance with very small $ITAE_d$ and T_{rcy}. The Lee-IMC method has a small M_{peak} but a very large T_{rcy}, while the SIMC method has a very large $ITAE_d$.

As shown in the Nyquist plots in Figure 14, the proposed PID controller has a similar MS_a value to the Lee-IMC controller, while the SIMC controller has the smallest MS_a value. However, all of them are within the range of MS_a values from 1.4 to 2.0 [34].

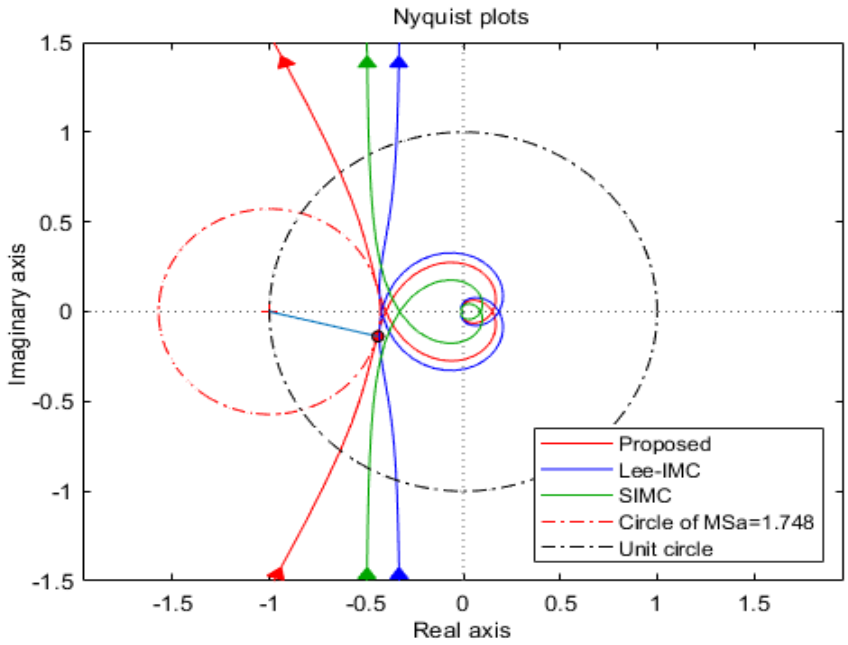

Figure 14. Nyquist plots and MS circle for the medium-speed region.

Considering all the performance indices, it can be concluded that the proposed method is superior to the other two methods.

4.2. Low-Speed Operating Region

To investigate the robustness of the controller to changes in the GT engine parameters, the controller designed in the medium-speed region is still used to simulate the TOPTD GT system in the low-speed region. In this case, the GT exhibits an increase of approximately 4% in steady-state gain compared to the nominal state condition. Additionally, the time delay increases by about 40.8%, and the time constant increases by approximately 42.3%.

Figure 15 shows the response when a step input of 1600 rpm is applied at t = 0 s, starting from an initial condition with the LPT rotating at 1000 rpm. Additionally, at t = 20 s, a disturbance input is introduced. In this scenario, the disturbance assumes that wind corresponding to 30% of the current load is applied as a step input in a vertical manner to the bow of the naval vessel. When operating at 1000 rpm, the position of the FMV spool is approximately 7.98 mm. Therefore, using Figure 9 to convert the current load to fuel flow rate, it corresponds to approximately 1380 kg/h, and external disturbances due to wind result in an additional fuel oil quantity of about 414 kg/h.

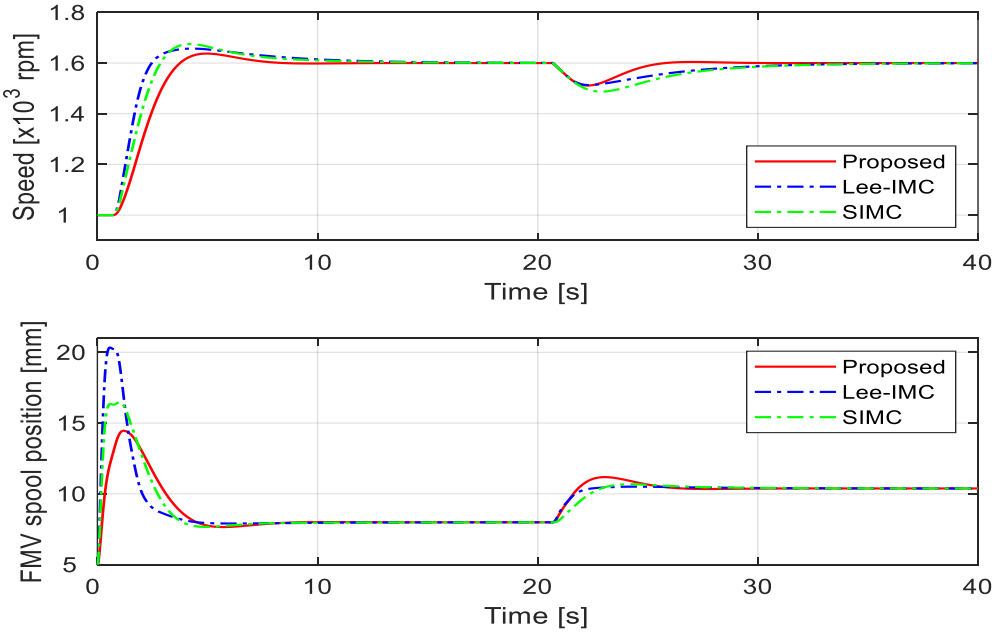

Figure 15. Step responses and FMV spool position for the low-speed region.

Table 6 summarizes the performance indices for the proposed controller and the controllers used for comparison.

Table 6. Performance comparisons for the low-speed operating region.

Tuning Methods	Tracking Performance			Disturbance Performance			MSa
	T_s	M_{peak}	$ITAE_s$	T_{rcy}	M_{peak}	$ITAE_d$	
Proposed	6.983	37.406	2069.6	8.777	88.64	714.6	1.846
SIMC	9.583	75.095	2955.1	16.151	112.8	2972.9	1.620
Lee-IMC	10.700	57.050	2974.5	16.752	87.43	2393.1	1.615

In the set-point tracking response, the proposed controller exhibits the smallest T_s, M_{peak}, and $ITAE_s$ values, making it superior in terms of all the performance indices. The Lee-IMC method has relatively larger $ITAE_s$ and T_s values. The SIMC method shows the largest M_{peak} value. In the disturbance rejection response, the proposed controller demonstrates significantly lower $ITAE_d$ and T_{rcy} values, showcasing excellent performance.

As seen in the Nyquist plots and MS circle in Figure 16, the Lee-IMC controller and the SIMC controller exhibit similar MS_a values, with both having smaller MS_a values than the proposed controller. However, all MS_a values are within the recommended range of 1.4 to 2.0 [34], ensuring good robustness.

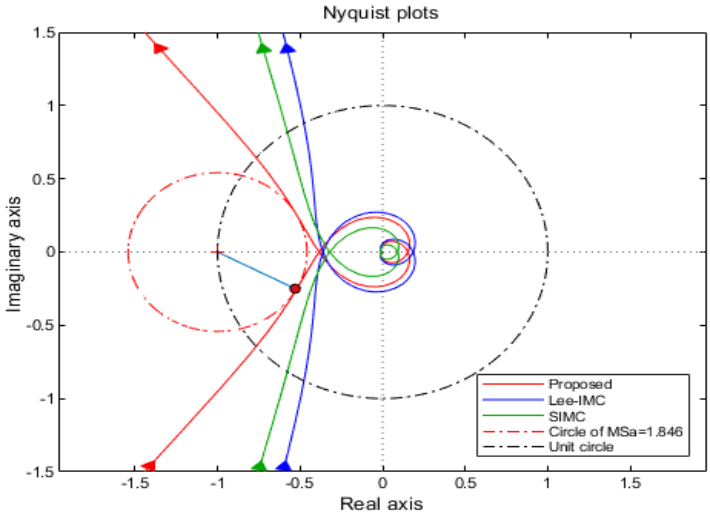

Figure 16. Nyquist plots and MS circle for the low-speed region.

Considering the overall performance in both set-point tracking and disturbance rejection, it can be concluded that the proposed method is superior to the other two methods.

4.3. High-Speed Operating Region

This time, the proposed controller is used to simulate the GT system in the high-speed region. In this case, the GT exhibits a decrease of approximately 8.3% in steady-state gain compared to the nominal state condition. Additionally, the time delay decreases by about 42.9%, and the time constant decreases by approximately 42.1%.

Figure 17 illustrates the response when a step input of 2800 rpm is applied at t = 0 s, starting from an initial condition with the LPT rotating at 2200 rpm. Additionally, at t = 20 s, a disturbance input is introduced.

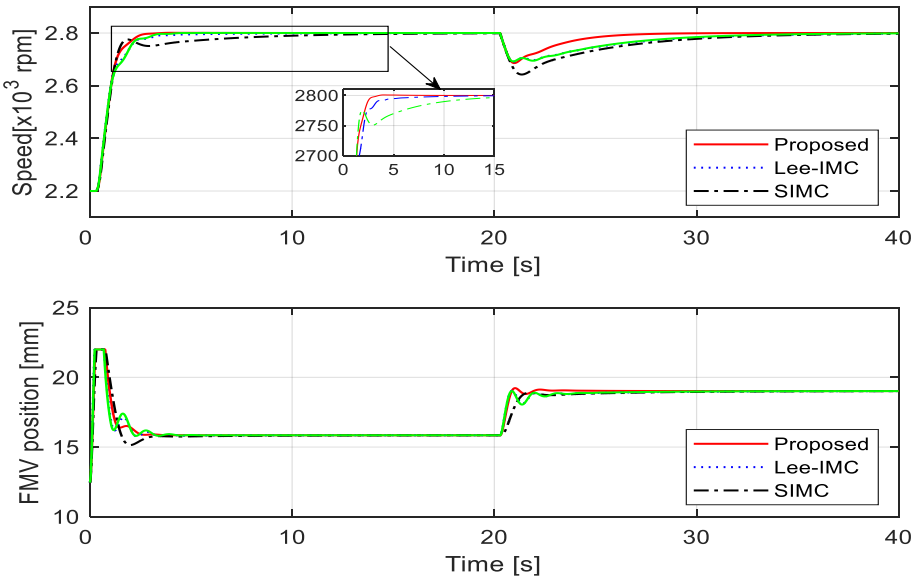

Figure 17. Step responses and FMV spool position for the high-speed range.

In this case, the disturbance assumes that, due to the current high load condition, wind equivalent to 20% of the current load is applied as a step input vertically to the bow of the naval vessel.

When operating at 2800 rpm, the position of the FMV spool is approximately 15.85 mm. Therefore, using Figure 9 to convert the current load to fuel flow rate, it corresponds to

approximately 3955 kg/h, and external disturbances due to wind result in an additional fuel oil quantity of about 791 kg/h.

Table 7 summarizes the performance indices for the proposed controller and the comparative controllers.

Table 7. Performance comparisons for the high-speed operating region.

Tuning Methods	Tracking Performance			Disturbance Performance			MSa
	T_s	M_{peak}	$ITAE_s$	T_{rcy}	M_{peak}	$ITAE_d$	
Proposed	2.378	0.881	371.7	8.577	114.2	753.9	1.949
SIMC	9.259	0.015	2061.5	17.160	156.7	4065.2	1.640
Lee-IMC	3.238	0.002	700.5	19.461	108.6	3250.8	2.278

As seen in Figure 17 and Table 7, in the set-point tracking response, the proposed controller exhibits the smallest $ITAE_s$ and T_s values. The Lee-IMC method has the smallest M_{peak} value but relatively larger $ITAE_s$ and T_s values. The SIMC method shows the largest $ITAE_s$ and T_s values. In all three methods, it can be observed that, in the set-point tracking response, the initial input is too large, causing the displacement of the FMV spool to reach the limit of 22 mm. In the disturbance rejection response, the proposed controller demonstrates significantly smaller $ITAE_d$ and T_{rcy} values, showcasing excellent performance.

As shown in the Nyquist plots and MS circle in Figure 18, the SIMC controller has the smallest MS_a, while the proposed controller has a moderate level of MS_a, but both methods fall within the recommended range [34]. However, the Lee-IMC controller has the largest MS_a with a value of 2.278, which falls outside the recommended range.

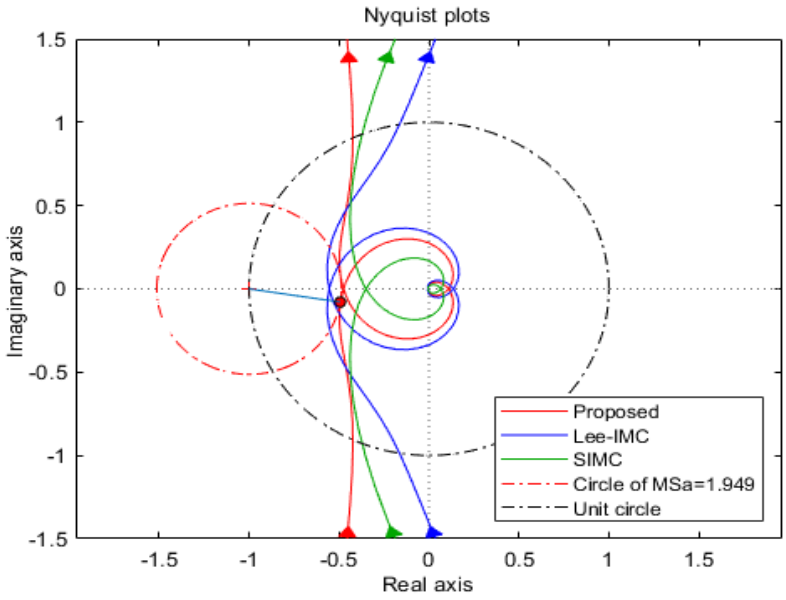

Figure 18. Nyquist plots and MS circle for the high-speed region.

Considering the overall performance in both set-point tracking and disturbance rejection, it can be concluded that the proposed method is superior to the other two methods.

4.4. Parameter Change

In general, the control problem becomes challenging when the process gain and time delay increase while the time constant decreases. Therefore, to assess the robustness of the controller, simulations are conducted assuming a 5% increase in both the gain K_E and time delay L_E and a 5% decrease in the time constant T_E compared to the model in the medium-speed region.

Figure 19 represents the response when a step input of 2200 rpm is applied at t = 0 s while the LPT is initially rotating at 1600 rpm, and then, a disturbance input is introduced at t = 20 s. In this case, the disturbance is assumed to be a step input perpendicular to the bow of the naval vessel, equivalent to 30% of the current load. In the current operating state, the position of the FMV spool is approximately 10.9 mm. Converting the current load to a fuel flow rate using Figure 9 results in approximately 2133 kg/h. The disturbance represents an additional fuel oil quantity of approximately 640 kg/h due to the influence of the wind.

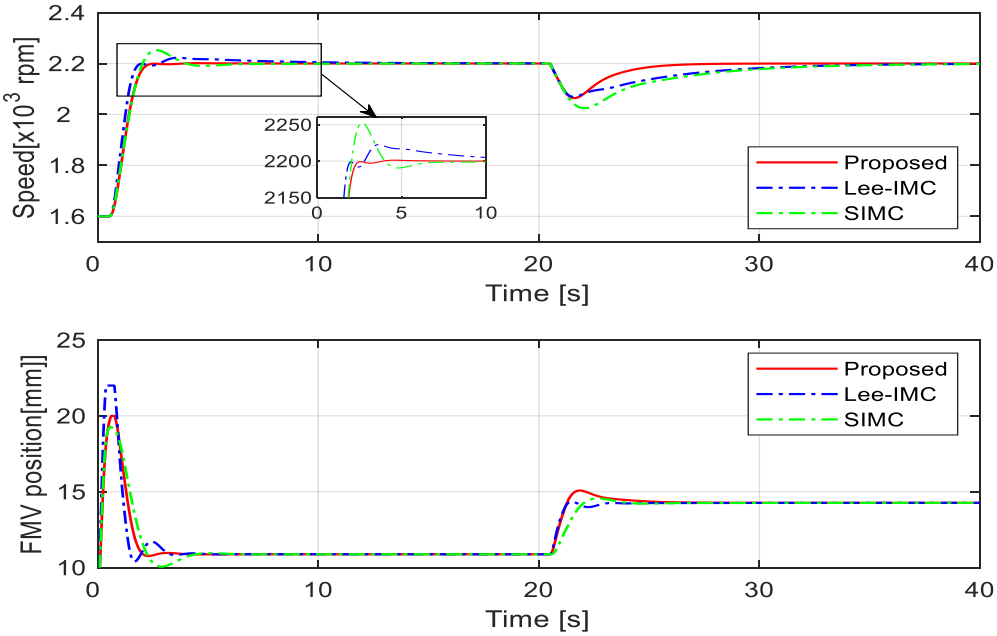

Figure 19. Step responses and FMV position for 5% parameter uncertainty.

Table 8 summarizes the performance indices for the proposed controller and the comparison controllers. As shown in Figure 19 and Table 8, in the set-point tracking response, the proposed controller exhibits superior performance in all performance indices, with the lowest values for $ITAE_s$, T_s, and M_{peak}. The Lee-IMC method has very large $ITAE_s$ and T_s values, while the SIMC method has a very high M_{peak} value. In particular, for Lee-IMC, it can be observed that, in the set-point tracking response, the initial input is too large, causing the displacement of the FMV spool to reach the limit of 22 mm. In disturbance rejection response, the proposed controller shows excellent performance with significantly low $ITAE_d$ and T_{rcy} values.

Table 8. Performance comparisons for 5% parameter change.

Tuning Methods	Tracking Performance			Disturbance Performance			MSa
	T_s	M_{peak}	$ITAE_s$	T_{rcy}	M_{peak}	$ITAE_d$	
Proposed	2.153	1.277	556.2	7.206	135.6	785.2	1.941
SIMC	3.679	52.311	873.7	17.434	175.3	4205.1	1.741
Lee-IMC	7.585	27.251	1495.3	17.797	131.1	3386.7	1.929

As shown in the Nyquist plots and MS circle in Figure 20, the MS_a of the SIMC controller is the smallest. The proposed controller and the Lee-IMC controller have similar levels of MS_a, but all three methods fall within the recommended range [34].

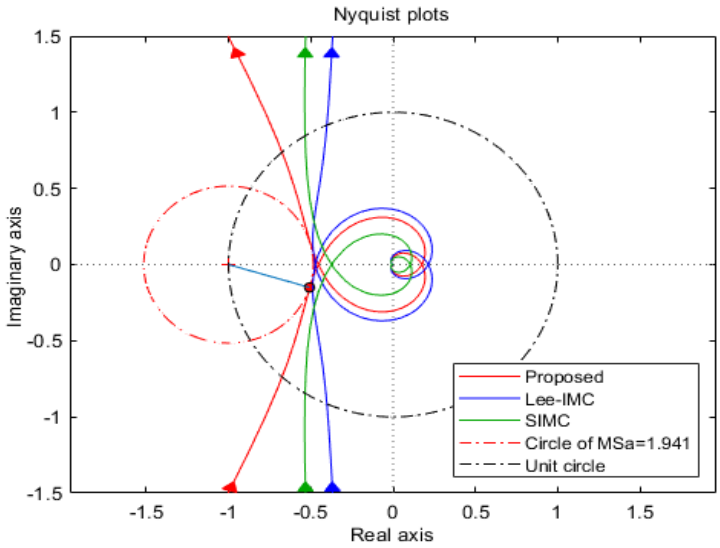

Figure 20. Nyquist plots and MS circle for 5% parameter uncertainty.

In conclusion, considering all aspects, it can be determined that the proposed method is superior to the other two methods.

5. Conclusions

This paper proposed a novel CEM-based 2-DOF PID controller for LPT speed control in the LM2500 gas turbine. The 2-DOF controller consists of a linear PID controller focused on disturbance rejection and a set-point filter to mitigate overshoot in the tracking performance. When tuning the PID controller, the maximum sensitivity, commonly used as a stability metric, is considered to maintain an appropriate balance between system stability and response performance. The key contributions of this paper are as follows:

- The LM2500 gas turbine exhibits significant parameter variations with respect to its rotational speed, so the entire rotational speed range is divided into three regions, and operational data from gas turbines installed on naval vessels are used to model each region.
- A novel approach called the characteristic equation matching method is proposed for controller design.
- By selecting a desired characteristic equation with multiple poles, there is only one adjustable variable for tuning the gains of the PID controller, making it easier for users to tune the controller.
- The use of a set-point filter is introduced to improve the tracking performance.
- Considering maximum sensitivity, the proposed controller ensures an appropriate level of system stability.

To validate the feasibility of the proposed controller, simulations were conducted over a wide range of operating speeds for the LPT of the LM2500 gas turbine. The simulation results showed that the proposed method achieved approximately 49% and 21.6–26.9% lower *ITAE* compared to the other two methods in the nominal state set-point tracking and disturbance rejection simulations, respectively. In the low-speed region simulations, the proposed method showed approximately 70% and 24–29.9% lower *ITAE*, and in the high-speed region simulations, it showed approximately 18–53% and 18.5–23.2% lower *ITAE* compared to the other two methods, respectively. Additionally, in the set-point tracking and disturbance rejection simulations with parameter variations, the proposed method showed approximately 45.8-63.6% and 18.7–23.2% lower *ITAE* compared to the other two methods, respectively. Therefore, considering all aspects comprehensively, the proposed method was significantly superior to the two other benchmark methods. Future research plans include designing controllers for each of the three operating regions and integrating them into a single controller.

Funding: This research was funded by the National Research Foundation of Korea (NRF), grant funded by the Korea government (No. RS-2022-00166517).

Data Availability Statement: The data presented in this study are available on request from the corresponding author.

Acknowledgments: The authors would like to thank the editor and the reviewers of this paper for their valuable comments that helped improve the quality of the paper.

Conflicts of Interest: The authors declare no conflicts of interest.

Nomenclature

CEM	Characteristic equation matching	K_D	Derivative gain
EEDI	Energy efficiency design index	K_E	Combustor-LPT system gain
FMU	Fuel oil metering unit	K_I	Integral gain
FMV	Fuel oil metering valve	K_L	LVDT gain
FOPTD	First-order plus time delay	K_p	Proportional gain
GA	Genetic algorithm	K_U	Transducer gain
GT	Gas turbine	K_V	FMV gain
HPT	High-pressure turbine	L	FOPTD model time delay
IMC	Internal model control	L_E	Combustor-LPT system time delay
IMO	International maritime organization	max	Maximum operator
$ITAE$, $ITAE_d$, $ITAE_s$	Integral of time-weighted absolute error	M_{peak}	Maximum peak error
LNG	Liquefied natural gas	$M(s)$	FOPTD model transfer function
LPG	Liquefied petroleum gas	$P_E(s)$	Combustor-LPT transfer function
LPT	Low-pressure turbine	$P_{FMU}(s)$	FMU transfer function
MPC	Model predictive control	$P_i(s)$, i = 1, 2, 3	Entire GT system transfer function
MS, MS_a, MS_d	Maximum sensitivity	PRC	Process reaction curve
NOx	Nitrogen oxides	$r(s)$	Reference input
SOx	Sulfur oxides	$r_f(s)$	Set-point filter output
PID	Proportional-integral-derivative	s	Laplacian variable
SMC	Sliding mode control	T	FOPTD model time constant
SOPTD	Second-order plus time delay	T_E	Combustor-LPT system time constant
TOPTD	Third-order plus time delay	T_{rcy}	Recovery time
VSVA	Variable stator vane actuator	T_s	Settling time
2-DOF	Two degrees of freedom	T_V	FMV time constant
$C(s)$	Controller transfer function	$u(s)$	Control input
$d(s)$	Disturbance input	w	Weighting factor
$e(s)$	Error	$y(s)$	LPT rotational speed, model output
$F_r(s)$	Set-point filter transfer function	$z(s)$	Spool displacement
$i(s)$	Amplifier output	λ	Adjustment variable
K	FOPTD model gain	ω	Angular frequency
K_A	Amplifier gain		

References

1. Rayaprolu, K. *Boilers for Power and Process*; CRC Press: Boca Raton, FL, USA, 2009.
2. Mohamed, O.; Wang, J.; Khalil, A.; Limhabrash, M. The application of system identification via canonical variate algorithm to North Benghazi gas turbine power generation system. In Proceedings of the 2015 IEEE Jordan Conference on Applied Electrical Engineering and Computing Technologies (AEECT), Amman, Jordan, 3–5 November 2015.
3. Rashid, K.; Sheha, M.N.; Powell, K.M. Real-time optimization of a solar-natural gas hybrid power plant to enhance solar power utilization. In Proceedings of the Annual American Control Conference (ACC), Milwaukee, WI, USA, 27–29 June 2018.
4. Roumeliotis, I.; Aretakis, N.; Alexiou, A. Industrial gas turbine health and performance assessment with field data. *ASME J. Eng. Gas Turbines Power* **2017**, *139*, 051202. [CrossRef]
5. Rivieramm. MT30 Gas Turbines Drive DDG-1000 Destroyers. 2008. Available online: https://www.rivieramm.com/news-content-hub/news-content-hub/mt30-gas-turbines-drive-ddg-1000-destroyers-51647 (accessed on 15 July 2024).
6. Lee, T.H.; Ki, J.Y.; Kho, S.H. Overview of the gas turbine status of the ship. In Proceedings of the 49th KSPE Fall Conference, Busan, Republic of Korea, 2 November 2017.

7. International Maritime Organization. IMO Marine Environment Protection Committee (MEPC) 75, 16–20 November (Virtual Session). 2020. Available online: https://www.imo.org/en/MediaCentre/MeetingSummaries/Pages/MEPC-75th-session.aspx (accessed on 15 July 2024).
8. International Maritime Organization. IMO Marine Environment Protection Committee 81st Session (MEPC81), 18–22 March 2024. 2024. Available online: https://www.imo.org/en/MediaCentre/MeetingSummaries/Pages/MEPC-81.aspx (accessed on 15 July 2024).
9. GE Aerospace. Two 30MW GE Gas Turbines Propel Queen Mary 2, the World's Largest Transatlantic Liner. 2017. Available online: https://www.geaerospace.com/sites/default/files/30mw-queen-mary-case-history.pdf (accessed on 15 July 2024).
10. Ship Technology. Francisco Papa High-Speed Ferry. 2013. Available online: https://www.ship-technology.com/projects/francisco-high-speed-ferry/ (accessed on 15 July 2024).
11. Direct Industry. Gas Turbine Catalog. 2006. Available online: https://pdf.directindustry.com/pdf/ge-gas-turbines//gas-turbines-catalog/34155-382967.html (accessed on 15 July 2024).
12. Rowen, W.I. Simplified mathematical representations of heavy-duty gas turbines. *ASME J. Eng. Gas Turbines Power* **1983**, *105*, 865–869. [CrossRef]
13. Hussain, A.; Seifi, H. Dynamic modeling of a single shaft gas turbine. In Proceedings of the IFAC Symposium on Control of Power Plants and Power Systems, Munich, Germany, 9–11 March 1992.
14. Yee, S.K.; Milanović, J.V.; Hughes, F.M. Validated models for gas turbines based on thermodynamic relationships. *IEEE Trans. Power Syst.* **2011**, *26*, 270–281. [CrossRef]
15. Chaibakhsh, A.; Amirkhani, S. A simulation model for transient behaviour of heavy-duty gas turbines. *Appl. Therm. Eng.* **2018**, *132*, 115–127. [CrossRef]
16. Cha, S.W.; Ki, J.Y.; Son, N.Y.; Kim, D.J.; Shim, J.S.; Kim, M.H.; Park, S.G. Development of a dynamic simulation mathematical model of a 2-spool marine gas turbine engine. *J. Korean Soc. Mar. Eng.* **2019**, *43*, 655–660.
17. Mohamed, O.; Za'ter, M.E. Comparative study between three modeling approaches for a gas turbine power generation system. *Arab. J. Sci. Eng.* **2020**, *45*, 1803–1820. [CrossRef]
18. Aygun, H.; Turan, O. Application of genetic algorithm in exergy and sustainability: A case of aero-gas turbine engine at cruise phase. *Energy* **2022**, *238*, 121644. [CrossRef]
19. Xu, M.; Liu, J.; Li, M.; Geng, J.; Wu, Y.; Song, Z. Improved hybrid modeling method with input and output self-tuning for gas turbine engine. *Energy* **2022**, *238*, 121672. [CrossRef]
20. Yang, Y.; Nikolaidis, T.; Jafari, S.; Pilidis, P. Gas turbine engine transient performance and heat transfer effect modelling: A comprehensive review, research challenges, and exploring the future. *Appl. Therm. Eng.* **2024**, *236*, 121523. [CrossRef]
21. Qin, S.J.; Badgwell, T.A. A survey of industrial model predictive control technology. *Cont. Eng. Pract.* **2003**, *11*, 733–764. [CrossRef]
22. Sáez, D.; Milla, F.; Vargas, L.S. Fuzzy predictive supervisory control based on genetic algorithms for gas turbines of combined cycle power plants. *IEEE Trans. Energy Convers.* **2007**, *22*, 689–696. [CrossRef]
23. Hou, G.L.; Gong, L.J.; Dai, X.Y.; Wang, M.Y.; Huang, C.Z. A novel fuzzy model predictive control of a gas turbine in the combined cycle unit. *Complexity* **2018**, 6468517. [CrossRef]
24. Bonfiglio, A.; Cacciacarne, S.; Invernizzi, M.; Lanzarotto, D.; Palmieri, A.; Procopio, R. A sliding mode control approach for gas turbine power generators. *IEEE Trans. Energy Convers.* **2019**, *34*, 921–932. [CrossRef]
25. Mohamed, O.; Khalil, A. Progress in Modeling and Control of Gas Turbine Power Generation Systems: A Survey. *Energies* **2020**, *13*, 2358. [CrossRef]
26. Zhou, X.; Lu, F.; Zhou, W.; Huang, J. An improved multivariable generalized predictive control algorithm for direct performance control of gas turbine engine. *Aerosp. Sci. Technol.* **2020**, *99*, 105576. [CrossRef]
27. Hou, G.; Gong, L.; Huang, C.; Zhang, J. Fuzzy modeling and fast model predictive control of gas turbine system. *Energy* **2020**, *200*, 117465. [CrossRef]
28. Lin, P.; Du, X.; Shi, Y.; Sun, X.M. Modeling and controller design of a micro gas turbine for power generation. *ISA Trans.* **2022**, *124*, 411–426. [CrossRef]
29. Ryu, K.T. GA-based Fuzzy-PID controller for LM-2500 gas turbine. Ph.D. Thesis, Graduate School Korea Maritime and Ocean University, Busan, Republic of Korea, 2023.
30. Lee, C.H.; Lee, Y.H.; Lee, C.S.; Ryu, K.T.; Zhao, H.Y.; So, M.O. Study on speed control of LM-2500 engine using IMC-LPID controller. *J. Korea Acad.-Ind.* **2022**, *23*, 984–993.
31. Skogestad, S. Simple analytic rules for model reduction and PID controller tuning. *J. Process Control* **2003**, *13*, 291–309. [CrossRef]
32. Mathworks. Curve Fitting Toolbox. 2021. Available online: https://www.mathworks.com/help/curvefit/ (accessed on 15 July 2024).
33. Elakkiya, T.; Priyanka, R. Comparative study of PID, IMC and IMC based PID controller for pressure process. *J. Chem. Pharm. Sci.* **2015**, 32–38.
34. Anil, C.; Sree, R.P. Tuning of PID controllers for integrating systems using direct synthesis method. *ISA Trans.* **2015**, *57*, 211–219. [CrossRef] [PubMed]